# MMSE Equalization for FBMC Transmission over Doubly-Selective Channels

Ljiljana Marijanović[†‡], Stefan Schwarz[†‡] and Markus Rupp[†]
[†] Institute of Telecommunications, Technische Universität (TU) Wien
[‡] Christian Doppler Laboratory for Dependable Wireless Connectivity for the Society in Motion
Email: {ljiljana.marijanovic,sschwarz,mrupp}@nt.tuwien.ac.at

***Abstract*—This paper presents a linear minimum mean square error (MMSE) equalizer for Filter bank Multicarrier (FBMC) systems for the equalization of fast-fading frequency-selective channels. Since FBMC employs Offset Quadrature Amplitude Modulation (OQAM), we consider a fractionally spaced per-subcarrier equalizer. This equalizer takes into account the interference from neighbouring subcarriers due to frequency selectivity of the channel and also the interference from adjacent symbols in time. Hence, the extended MMSE equalizer for fast fading scenarios is derived and we evaluate its performance in terms of equalizer length, number of neighbouring symbols, different mobility and we compare it to a simple one-tap equalizer.**

***Index Terms*—Linear minimum mean square error equalization, fast fading, FBMC, symbol error ratio**

## I. Introduction

Many wireless communication systems employ multicarrier modulation to support highest data rates over transmission channels that are selective in time and frequency. So far the most investigated technique, cyclic prefix-based orthogonal frequency division multiplexing (CP-OFDM), has offered great improvements, but new applications still strive to gain better properties in terms of data rate, spectral agility, robustness and reliability [1], [2]. The next potential solution is filter bank multicarrier (FBMC) modulation, one of the contenders for 5G. It offers many advantages compared to CP-OFDM in terms of spectrum utilization, capacity and user mobility [1], [2], [3],[4]. However, FBMC requires comparatively complex equalization techniques. Due to the absence of redundancy (cyclic prefix), a simple one-tap equalization is not sufficient to cope with frequency-selective channels, and in particular to deal with doubly-selective channels.

Many papers are dealing with equalization in FBMC, but mainly provide solutions in the case of frequency-selective channels. Linear minimum mean square error (MMSE) per subcarrier equalization for frequency-selective block-fading channels is described in [5]. The authors present a system model which takes into account only the strongest intercarrier interference (ICI) coming from adjacent subcarriers. There is also an extended version of this approach in [4], enhancing [5] to multiple band MMSE equalization. This is achieved by employing not only outputs of immediately adjacent subcarriers, but rather considering outputs of many neighboring subcarriers. The problem of channel equalization with a nonlinear MMSE decision feedback equalizer is considered in [6]. MMSE-frequency spreading equalization (FSE) for massive MIMO is explained in [7]. The method leads to a more accurate equalization allowing to transmit a higher number of bits per symbol and to extend the bandwidth of each subcarrier. This spectral broadening of subcarriers provides a lot of benefits, such as, reduced peak-to-average power ratio, robustness to frequency offset, lower complexity and reduced latency [7]. The effect of intersymbol intereference originating from non-completely equalized channels in precoded FBMC using linear MMSE equalization is analysed in [8]. The intersymbol interference (ISI) causes a loss of diversity. The authors proposed to use subchannel equalizers with multiple taps or a larger number of subcarriers to prevent the loss of diversity. In [9] a comparison of a maximum likelihood sequence estimator (MLSE) and MMSE subchannel equalization is provided.

FBMC is based on Offset-Quadrature-Amplitude-Modulation (OQAM) which allows efficient use of the spectrum, but also gives some implications on the structure of FBMC. The FBMC design we employ relies on Physical Layer For Dynamic Spectrum Access And Cognitive radio (PHYDYAS) structure described in [10]; however, our approach is generally applicable to other waveforms as well.

### A. Notation

In the upcoming sections we use the following notation: By $\otimes$ we denote the Kronecker product, by $\lceil\cdot\rceil$ the real value is mapped to the smallest following integer (ceiling function). The Hadamard product we denote by $\circ$. If we write $[\mathbf{X}]_{i:i',j:j'}$, it means that we take only the part of matrix $\mathbf{X}$, from $i$-th to $i'$-th row and from $j$-th from $j'$-th column. Furthermore, we use $[\mathbf{X}_k]_{i,j}$ to denote specific elements of matrix $\mathbf{X}_k$, $i$-th row and $j$-th column, corresponding to subcarrier $k$.

## II. System Model

The structure of FBMC is depicted in Figure 1. It is characterized by a PHYDYAS prototype filter and the polyphase structure of a synthesis filter bank (SFB) and an analysis filter bank (AFB) as well as OQAM pre-processing and OQAM post-processing blocks. The fractionally spaced per-subcarrier equalizer is inserted before the OQAM post-processing which means that it operates at double symbol rate $2/T$, with $1/T$ denoting the symbol rate.

The first block represents the OQAM pre-processing; it is further detailed in Figure 2. This block presents a conversion from the complex to either the real or imaginary domain by

978-1-5090-2061-4/16/$31.00 ©2016 IEEE

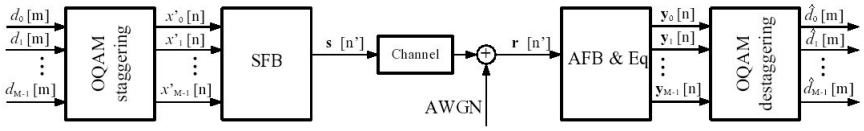


Figure 1: Structure of FBMC.

dividing complex-valued symbol $d_k[m] = a_k[m] + jb_k[m]$ into the two new symbols $a_k[m]$ and $b_k[m]$. The index $k$ is the subcarrier index and index $m$ is the time index at symbol rate $T$. As a result we obtain purely real and imaginary symbols in the output $x'_k[n]$ where the symbol rate is increased by a factor of 2, which is represented by index $n$. The order of the real and imaginary symbols is not always the same. It depends on the parity of the subcarrier index $k$ depicted in Figure 2. This operation is also called staggering. The next block is the SFB which is composed of $M$ upsamplers and $M$ synthesis filters. Each of these filters is obtained from the zero-phase prototype filter $h_0[l]$ with length $L_p = KM + 1$ by applying exponential modulation.

$$h_k[l] = h_0[l]\exp(j2\pi kl/M) \tag{1}$$

where $l = -KM/2, ..., KM/2$ is the time index, $K$ is the overlapping factor and $M$ is the total number of subcarriers. The overlapping factor $K$ determines the ratio of the filter impulse response duration to the symbol period. In the other words, it is the number of overlapped symbols in the time. At the output of the SFB, there is a high rate signal which is composed of low rate subcarrier signals. The low rate subcarrier signals are summed up to obtain the transmit signal. To describe the input-output relationship of the system, we consider a block-based transmission with transmit blocks of length $N$. The transmit signal at the output of the SFB is:

$$\mathbf{s}_k[n'] = \mathbf{M}_k\ \mathbf{S}\ \mathbf{U}\ \mathbf{x}'_k[n] \tag{2}$$

where $\mathbf{s}_k[n'] \in \mathbb{C}^{L_p+N\frac{M}{2}-1}$ and $n'$ is the sample time index after the upsampling block $\mathbf{U} = \mathbf{I}_N \otimes \mathbf{e}_1$. Here, $\mathbf{I}_N$ denotes the size $N \times N$ identity matrix and $\mathbf{e}_1$ is the canonical basis vector of length $M/2$: $[1, 0, ..., 0]^T$. The vector $\mathbf{x}'_k[n] \in \mathbb{C}^N$ contains the block of $N$ transmit symbols obtained after OQAM preprocesssing:

$$\mathbf{x}'_k[n] = [\ \ x'_k[n], x'_k[n-1], ..., x'_k[n-N+1]\ \ ]^T \tag{3}$$

with $N$ denoting the transmit block length, i.e., the total number of OQAM symbols.

Matrix $\mathbf{M}_k \in \mathbb{C}^{\left(L_p+N\frac{M}{2}-1\right)\times\left(L_p+N\frac{M}{2}-1\right)}$ represents the modulation of subcarrier $k$:

$$\mathbf{M}_k = \mathrm{diag}\left(e^{\left(j\frac{2\pi k}{M}\left[0,1...,(L_p+\frac{M}{2}N-1)\right]\right)}\right). \tag{4}$$

Matrix $\mathbf{S} \in \mathbb{C}^{\left(L_p+N\frac{M}{2}-1\right)\times N\frac{M}{2}}$ performs the convolution with the prototype filter impulse response $h_0[l]$.

The sum of the subcarrier signals is transmitted over a doubly-selective channel where additive white Gaussian noise (AWGN) is added as given in (5). The channel is not only frequency selective (time dispersive), but also time selective (frequency dispersive). Our equalizer compensates for both: multipath propagation and temporal channel variation.
The receive signal after the channel is obtained as:

$$\mathbf{r}[n'] = \mathbf{H}[n'] \sum_{k=0}^{M-1} \mathbf{s}_k[n'] + \boldsymbol{\eta}_k[n'] \in \mathbb{C}^{L_{ch}+L_p+N\frac{M}{2}-1}, \tag{5}$$

where $\mathbf{H}[n'] \in \mathbb{C}^{\left(L_{ch}+L_p+N\frac{M}{2}-1\right)\times\left(L_p+N\frac{M}{2}-1\right)}$ is the channel matrix and $L_{ch}$ is the number of channel taps. The channel matrix is shown in (6), where $h_{ch}$ are the channel coefficients with the first index corresponding to the time (symbol) position and the second index corresponding to the current channel delay tap. The vector $\boldsymbol{\eta}_k[n']$ presents complex Gaussian noise with zero mean and variance $\sigma^2_\eta$.

The AFB is composed of analysis filters that are time-reversed and complex-conjugated versions of the synthesis filters. At the receiver side there are $M$ downsamplers and $M$ filters.
The signal corresponding to subcarrier $k$ at the output of the AFB is given below:

$$\mathbf{y}_k[n] = \mathbf{V}\ \mathbf{A}\ \mathbf{D}_k\ \mathbf{r}[n'] \tag{7}$$

where $\mathbf{V} = (\mathbf{I}_{\lceil\frac{p}{M/2}\rceil} \otimes \mathbf{e}_1^T)_{:,1:p}$ is the downsampling block, $\mathbf{A} \in \mathbb{C}^{p\times\left(L_{ch}+L_p+N\frac{M}{2}-1\right)}$ is the analysis matrix and $p = \left(L_{ch} + 2L_p + N\frac{M}{2} - 3\right)$ corresponds to the number of rows of matrix $\mathbf{A}$.

Matrix $\mathbf{D}_k \in \mathbb{C}^{\left(L_{ch}+L_p+N\frac{M}{2}-1\right)\times\left(L_{ch}+L_p+N\frac{M}{2}-1\right)}$ is the demodulation matrix of subcarrier:

$$\mathbf{D}_k = \mathrm{diag}\left(e^{\left(-j\frac{2\pi k}{M}\left[0,1,...,(L_{ch}+L_p\frac{M}{2}N-1)\right]\right)}\right) \tag{8}$$

The size of the matrices in the present system model depends on the considered block-length $N$; hence, computational complexity for determining these matrices grows quadratically with $N$. In the following, we derive an equivalent input-ouput relationship, in which we combine all elements of the transceiver chain into a single matrix multiplication. We furthermore show that the elements of this matrix can be calculated with a complexity that basically depends on the length of the prototype filter $L_p$ and does not grow with $N$. We will then utilize this model in Sec. III to determine the

$$\begin{bmatrix} h_{ch}[n',0] & h_{ch}[n'-1,1] & \dots & h_{ch}[n'-L_{ch}+1,L_{ch}] & 0 & \dots & \dots \\ 0 & h_{ch}[n'-1,0] & h_{ch}[n'-2,1] & \dots & \dots & 0 & \dots \\ \vdots & \vdots & \vdots & \ddots & \vdots & \vdots & \vdots \\ 0 & \dots & \dots & \dots & 0 & h_{ch}[n'-N+1,0] & h_{ch}[n'-N+1,1] \\ 0 & \dots & \dots & \dots & \dots & 0 & h_{ch}[n'-N,0] \end{bmatrix} \tag{6}$$

MMSE equalizer for the considered doubly-selective channel. Our goal is to derive an input-output relationship of the form:

$$\mathbf{y}_k[n] = \mathbf{H}_k^{\text{eff}}[n]\mathbf{x}'_k[n] + \sum_{k' \neq k} \mathbf{H}_{k,k'}^{\text{eff}}[n]\mathbf{x}'_{k'}[n] + \boldsymbol{\eta}_{T,k}[n] \tag{9}$$

with $\mathbf{H}_k^{\text{eff}}[n]$ denoting the effective channel and $\boldsymbol{\eta}_{T,k}[n]$ representing the filtered noise after demodulation, analysis filter and downsampler. The second part of the equation represents the ICI components that corresponding to the effective interference channels $\mathbf{H}_{k,k'}^{\text{eff}}[n]$ and $\mathbf{x}'_{k'}[n]$ are the input symbols corresponding to the subcarrier index $k'$. The effective channel has the following structure:

$$\mathbf{H}_k^{\text{eff}}[n] = \mathbf{V}\ \tilde{\mathbf{H}}_k[n']\ \mathbf{U} \tag{10}$$

with $\mathbf{U}$ denoting the upsampling part and $\mathbf{V}$ denoting the downsampling part, respectively. The matrix $\tilde{\mathbf{H}}_k[n']$ is composed of the analysis matrix, the demodulation matrix, the channel, the modulation matrix and the synthesis matrix in this order:

$$\tilde{\mathbf{H}}_k[n'] = \mathbf{A}\ \mathbf{D}_k\ \mathbf{H}[n']\ \mathbf{M}_k\ \mathbf{S} \tag{11}$$

To efficiently calculate the entries of matrix $\mathbf{H}_k^{\text{eff}}[n]$, we can exploit the structure of the upsampling and downsampling matrices. The $i,j$-th entry of matrix $\mathbf{H}_k^{\text{eff}}[n]$ is obtained as:

$$[\mathbf{H}_k^{\text{eff}}]_{i,j}[n] = [\mathbf{V}]_{i,:}\ \tilde{\mathbf{H}}_k[n']\ [\mathbf{U}]_{:,j}. \tag{12}$$

The column vectors and row vectors $\mathbf{U}_{:,j}$ and $\mathbf{V}_{i,:}$ contain only one single non-zero element at position $\tilde{j}$ and $\tilde{i}$, respectively:

$$\tilde{i} = (i-1)\frac{M}{2} + 1, \quad \tilde{j} = (j-1)\frac{M}{2} + 1. \tag{13}$$

Hence, the $i,j$-th entry of matrix $\mathbf{H}_k^{\text{eff}}[n]$ is obtained from the $\tilde{i},\tilde{j}$-th entry of matrix $\tilde{\mathbf{H}}_k[n]$.

$$[\mathbf{H}_k^{\text{eff}}]_{i,j}[n] = [\tilde{\mathbf{H}}_k]_{\tilde{i},\tilde{j}}[n] = \mathbf{A}_{\tilde{i},:}\mathbf{D}_k\,\mathbf{H}[n']\,\mathbf{M}_k\,\mathbf{S}_{:,\tilde{j}} \tag{14}$$

Notice that vector $\mathbf{S}_{:,\tilde{j}}$ contains only $L_p$ non-zero elements; we gather these elements in vector $\mathbf{s} \in \mathbb{C}^{L_p \times 1}$. Vector $\mathbf{A}_{\tilde{i},:}^T$ contains at most $L_p$ non-zero elements, depending on the selected row index $\tilde{i}$. We gather these $L_a$ elements in vector $\mathbf{a} \in \mathbb{C}^{L_a \times 1}$. Furthermore, we gather the corresponding $L_p$ and $L_a$ diagonal elements of matrices $\mathbf{D}_k$ and $\mathbf{M}_k$, respectively, in the vectors $\mathbf{d}_k$ and $\mathbf{m}_k$. Finally, we combine the relevant entries of matrix $\mathbf{H}[n']$, corresponding to these non-zero elements, in matrix $\mathbf{H}_r[n'] \in \mathbb{C}^{L_a \times L_p}$.

$$[\mathbf{H}_k^{\text{eff}}]_{i,j}[n] = (\mathbf{a} \circ \mathbf{d}_k)^T \mathbf{H}_r[n'](\mathbf{m}_k \circ \mathbf{s}). \tag{15}$$

Equation (15) thus describes how a fast-fading multipath channel impacts the FBMC transmission. Commonly $L_{ch}$ is much less than $L_p$ and hence most entries of $\mathbf{H}_r[n']$ are zero, which can be exploited to further reduce computational complexity.

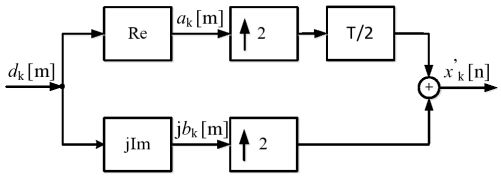


Figure 2: OQAM Staggering for k odd

According to this we can define our effective interference channel matrix:

$$[\mathbf{H}_{k,k'}^{\text{eff}}]_{i,j}[n] = (\mathbf{a} \circ \mathbf{d}_k)^T \mathbf{H}_r[n'](\mathbf{m}_{k'} \circ \mathbf{s}). \tag{16}$$

## III. Equalizer representation

In our equalizer, we consider the impact of ISI from $L\max$ past and previous symbols as well as ICI from immediately adjacent subcarriers. As we consider only neighbouring subcarriers, the corresponding input $\mathbf{y}'_k[n] \in \mathbb{C}^{N_{eq}}$ of the equalizer can be approximated by:

$$\begin{aligned}\mathbf{y}'_k[n] \approx\ & \mathbf{G}'_k[n]\mathbf{x}'_k[n] + \mathbf{Q}'_k[n]\mathbf{x}'_{k-1}[n] + \mathbf{Z}'_k[n]\mathbf{x}'_{k+1}[n] \\ & + \boldsymbol{\Gamma}_k[n]\boldsymbol{\eta}[n']\end{aligned} \tag{17}$$

where $\mathbf{G}'_k[n] \in \mathbb{C}^{\mathbf{N}_{eq} \times P}$, $\mathbf{Q}'_k[n] \in \mathbb{C}^{\mathbf{N}_{eq} \times P}$and $\mathbf{Z}'_k[n] \in \mathbb{C}^{\mathbf{N}_{eq} \times P}$ are matrices belonging to different subcarrier impulse responses [5]. Matrix $\mathbf{G}'_k$ is obtained from the appropriate elements of matrix $\mathbf{H}_k^{\text{eff}}[n]$, (15). Matrices $\mathbf{Q}'_k$ and $\mathbf{Z}'_k$ are obtained from the appropriate elements of ICI matrices of immediately adjacent subcarriers, $k-1$ and $k+1$, respectively, (16). Considering only frequency selective channels, these matrices are diagonal-constant but in the case of doubly-selective channels we have to account for variations from symbol to symbol. As a consequence, each row of these matrices has different values which corresponds to the current symbol time index as well as past symbol time indices. Equation (18) shows the example for $\mathbf{G}'_k[n]$, but this structure is valid for matrices $\mathbf{Q}'_k[n]$ and $\mathbf{Z}'_k[n]$. Matrix $\boldsymbol{\Gamma}_k[n]$ comprises the filtering of the noise with receive filter. We consider $L_{max}$ past and $L_{max}$ previous symbols in our equalizer. Hence, the length of the effective impulse is $L = 2L_{max} - 1$.

The transmit vector $\mathbf{x}'_k[n] \in \mathbb{C}^P$ with $P = N_{eq} + L - 1$ can be defined as:

$$\begin{aligned}\mathbf{x}'_k[n] = \Big[ & x'_k[n + L_{max}], \dots, x'_k[n], \dots, x'_k[n - L_{max}], \\ & \dots, x'_k[n + L_{max} - \nu], \dots, x'_k[n + L_{max} - P]\Big]^T.\end{aligned} \tag{19}$$

$$\mathbf{G}'_k[n] = \begin{bmatrix} g'_k[n,-L_{max}] & \dots & g'_k[n,L_{max}] & 0 & \dots & \dots & \dots & 0 \\ 0 & g'_k[n-1,-L_{max}] & \dots & g'_k[n-1,L_{max}] & 0 & \dots & \dots & 0 \\ \vdots & \vdots & \vdots & \vdots & \vdots & \vdots & \vdots & \vdots \\ 0 & 0 & \dots & \dots & \dots & \dots & 0 & g'_k[n-N_{eq},P] \end{bmatrix} \tag{18}$$

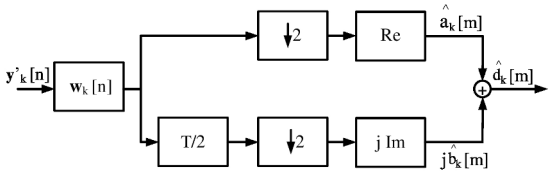


Figure 3: OQAM Destaggering.

with the position $\nu$ denoting the equalizer delay. It depends on the channel propagation and filters, and it is in the range of 0 to $P-1$.

The element we want to detect from vector $\mathbf{x}'_k[n]$ depends on the delay of the equalizer and on the subcarrier parity according to Table I.

Table I: The desired detecting position of the vector $\mathbf{x}'_k[n-\nu]$.

| $x'_k[n-\nu]$ | $\nu_{even}$ | $\nu_{odd}$ |
|---|---|---|
| $k_{even}$ | $a_k[m-\nu]$ | $jb_k[m-\nu]$ |
| $k_{odd}$ | $jb_k[m-\nu]$ | $a_k[m-\nu]$ |

In order to compute corresponding matrices for our equalizer every second column of matrices $\mathbf{G}'_k[n]$, $\mathbf{Q}'_k[n]$ and $\mathbf{Z}'_k[n]$ are multiplied by $j$, before taking the real and imaginary part in (25). This is done in order to cancel the imaginary part and obtain a purely real-valued transmit sequence. After multiplication we obtain new matrices: $\mathbf{G}_k[n]$, $\mathbf{Q}_k[n]$ and $\mathbf{Z}_k[n]$.
We can split the signal $\mathbf{y}'_k[n]$ into the new real and imaginary forms that is shown in (20) and (21):

$$\begin{aligned} \mathbf{y}'^{(R)}_k[n] &= \mathrm{Re}\Big[\mathbf{y}'_k[n]\Big] \approx \mathbf{G}^{(R)}_k[n]\mathbf{x}'_k[n] + \mathbf{Q}^{(R)}_k[n]\mathbf{x}_{k-1}[n] \\ &\quad + \mathbf{Z}^{(R)}_k[n]\mathbf{x}_{k+1}[n] + \mathrm{Re}\Big[\mathbf{\Gamma}_k[n]\boldsymbol{\eta}[n]\Big] \end{aligned} \tag{20}$$

$$\begin{aligned} \mathbf{y}'^{(I)}_k[n] &= \mathrm{Im}\Big[\mathbf{y}'_k[n]\Big] \approx \mathbf{G}^{(I)}_k[n]\mathbf{x}_k[n] + \mathbf{Q}^{(I)}_k[n]\mathbf{x}_{k-1}[n] \\ &\quad + \mathbf{Z}^{(I)}_k[n]\mathbf{x}_{k+1}[n] + \mathrm{Im}\Big[\mathbf{\Gamma}_k[n]\boldsymbol{\eta}[n]\Big]. \end{aligned} \tag{21}$$

When we filter the output signal of AFB $\mathbf{y}'_k[n]$ with the equalizer and apply the destaggering process that is shown in Figure 3, we estimate symbol $\hat{a_k}[m-\nu]$ as a real part and $\hat{b_k}[m-\nu]$ as imaginary part of the receive symbol at the desired position $\nu$. Our equalizer is intended to cope with both ICI as a consequence of temporal channel variation and ISI as a consequence of multipath propagation. The aim is to minimize the MSE between the estimated signal $\hat{d}_k[m-\nu] = \hat{a}_k[m-\nu] + j\hat{b}_k[m-\nu]$ and the input signal $d_k[m-\nu] = a_k[m-\nu] + jb_k[m-\nu]$. It can be expressed as:

$$\mathbf{w}_k[n] = \mathrm{Re}(\mathbf{w}_k[n]) + \mathrm{jIm}(\mathbf{w}_k[n]) = \mathbf{w}^{(R)}_k + \mathrm{j}\mathbf{w}^{(I)}_k \in \mathbb{C}^{N_{eq}\times 1} \tag{22}$$

with:

$$\begin{aligned} \mathbf{w}^{(R)}_k[n] &= \arg\min_{\mathbf{w}_k[n]} E\Big[\,\big|\hat{a}_k[m-\nu] - a_k[m-\nu]\big|^2\Big] \\ \mathbf{w}^{(I)}_k[n] &= \arg\min_{\mathbf{w}_k[n]} E\Big[\,\big|\hat{b}_k[m-\nu] - b_k[m-\nu]\big|^2\Big]. \end{aligned} \tag{23}$$

So far we have offered results separately, real and imaginary part, but it is important to emphasize that the final equalizer coefficients are complex-valued. The equalizer filter impulse response is produced avoiding ISI both for $a_k[m-\nu]$ and $b_k[m-\nu]$ in combination with staggering in both cases for $k$ odd and $k$ even. When we plug (20) and (21) into (23) and differentiate with respect to $\mathbf{w}^{(R)}_k$ and $\mathbf{w}^{(I)}_k$, we obtain:

$$\mathbf{w}'_k[n] = \Big[\mathbf{P}_k[n]\mathbf{R}_x[n]\mathbf{P}^T_k[n] + \mathbf{F}_k[n]\hat{\mathbf{R}}_x[n]\mathbf{F}^T_k[n] + \mathbf{R}'_{\eta,k}[n]\Big]^{-1}\mathbf{P}_k[n]\mathbf{R}_x\mathbf{e}_\nu \tag{24}$$

with

$$\mathbf{P}_k[n] = \begin{bmatrix} \mathbf{G}^{(R)}_k[n] \\ \mathbf{G}^{(I)}_k[n] \end{bmatrix}, \quad \mathbf{F}_k[n] = \begin{bmatrix} \mathbf{Q}^{(R)}_k[n] & \mathbf{Z}^{(R)}_k[n] \\ \mathbf{Q}^{(I)}_k[n] & \mathbf{Z}^{(I)}_k[n] \end{bmatrix}, \tag{25}$$

$$\mathbf{R}'_{\eta,k}[n] = \frac{\sigma^2_\eta}{2}\mathbf{\Gamma}'_k[n]\mathbf{\Gamma}'^T_k[n], \quad \mathbf{\Gamma}'_k[n] = \begin{bmatrix} \mathbf{\Gamma}^{(R)}_k[n] & \mathbf{\Gamma}^{(I)}_k[n] \\ \mathbf{\Gamma}^{(I)}_k[n] & -\mathbf{\Gamma}^{(R)}_k[n] \end{bmatrix}. \tag{26}$$

$\mathbf{R}_x$ is the correlation matrix of the stationary OQAM symbols with the variance $\sigma^2_d = \mathrm{E}\Big[d[m]\,d^*[m]\Big]$.

$$\mathbf{R}_x = \frac{1}{2}\boldsymbol{I}_{L+1}\sigma^2_d. \tag{27}$$

Vector $\mathbf{e}_\nu$ is defined as a unit vector with a single one at position $\nu$.
We apply a complex equalizer to our output signal before destaggering, Figure 3, combining the real and imaginary part of the obtained equalizer coefficients. The complex equalizer is the relation between $\mathbf{w}'_k$ in (24) and $\mathbf{w}_k$ in (23).

$$\mathbf{w}'^T_k[n] = [\mathbf{w}^{(R),T}_k[n], \mathbf{w}^{(I),T}_k[n]] \in \mathbb{R}^{2N_{eq}} \tag{28}$$

## IV. Simulation Results

In this work we presented MMSE equalization which is intended to cope with doubly-selective channels. In this context, we have performed many experiments to show how our equalizer behaves. The parameters we used are given in Table II. Figure 4 shows curves obtained by the application of

Table II: Parameters for simulations.

| Parameters | Values |
|---|---|
| Total number of subcarriers | 72 |
| Carrier frequency | 5.9GHz |
| Overlapping factor | 4 |
| Total number of transmit symbols | 30 |
| Channel Model | Typical urban |

the MMSE equalizer (28) with different modulation alphabets, starting from 2QAM up to 64QAM modulation with a velocity

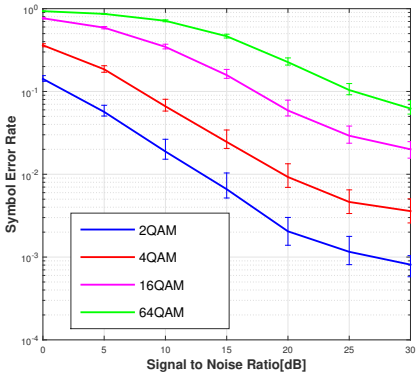


Figure 4: MMSE equalization using (28) for different modulation formats with $L_{max} = 3$ and $N_{eq} = 15$.

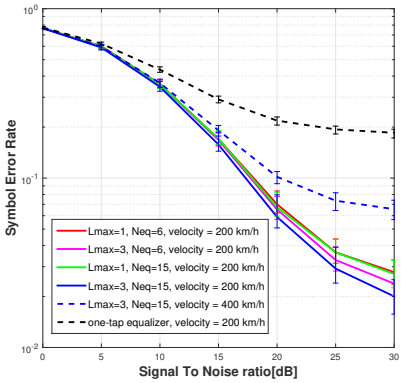


Figure 5: MMSE equalization for different lengths of equalizer and effective impulse response.

of 200 km/h. We show the dependance of symbol error ratio (SER) versus signal to noise ratio (SNR). In terms of SER we obtain what we expect: 2QAM modulation shows the best result while 64QAM is the worst case. Due to residual ICI SER saturates at large SNR and it is more pronounced with higher velocity. Figure 5 presents the impact of different lengths of the effective impulse response on our system as well as the impact of different lengths of the equalizer. The curves are obtained for the four cases employing 16QAM: in red we present the length of equalizer $N_{eq}$ = 6 considering only two neighbouring symbols, previous and following symbol; In magenta the case with the same equalizer length and with three symmetric neighbouring symbols is shown; The green and blue curves present the equalizer with the length $N_{eq} = 15$ and two cases with different effective impulse responses mentioned previously, respectively. From this figure it can be concluded that the more neighbouring symbols we take into account, the better is the result we have. Also, with too small $L_{max}$ even with different lengths of the equalizer, we have pretty similar results. However, increasing $L_{max}$, the impact of equalizer length is more pronounced. The black dash curve represents a one-tap equalizer which is not so sufficient to cope with ICI and ISI successively and because of that it shows worse characteristics than an MMSE equalizer. Also, we show the impact of different velocities on the system, regarding our equalizer is proposed for higher mobility. The curves depicted previously is obtained for a velocity of 200 km/h. We also have repeated the experiment with the best performance (blue curve) with a velocity of 400 km/h. As it is mentioned before, due to the residual ICI that cannot be removed by an MMSE equalizer, there is an error floor at larger SNR values (cyan curve) and it is more pronounced with smaller equalizer length and considered $L_{max}$.

## V. Conclusion

In this paper we derived MMSE equalization that is able to cope with doubly-selective channels considering most influential interferers: neighbouring subcarriers in the frequency domain and more neighbouring symbols in the time domain. The implemented MMSE equalizer is robust against time-variant channel even for high mobility. This is particularly pronounced compared to one-tap equalizer that is able to overcome neither ICI nor ISI. Increasing the length of equalizer means slightly increasing computational complexity, but at the same time it means better SER performance especially if it is combined with the larger effective impulse response length.

**Acknowledgment:**The financial support by the Austrian Federal Ministry of Science, Research and Economy and the National Foundation for Research, Technology and Development is gratefully acknowledged.

## References

[1] B. D. Tensubam, N. L. Chanu, and S. Singh, "Comparative analysis of FBMC and OFDM multicarrier techniques for wireless communication networks," *International Journal of Computer Applications*, vol. 100, no. 19, 2014.

[2] A. Farhang, N. Marchetti, F. Figueiredo, and J. P. Miranda, "Massive MIMO and waveform design for 5th generation wireless communication systems," pp. 70–75, 2014.

[3] H. Zhang, D. L. Ruyet, D. Roviras, and H. Sun, "Capacity analysis of OFDM/FBMC based cognitive radio networks with estimated CSI," pp. 1–5, 2010.

[4] M. Bellanger, D. Le Ruyet, D. Roviras, M. Terré, J. Nossek, L. Baltar, Q. Bai, D. Waldhauser, M. Renfors, T. Ihalainen *et al.*, "FBMC physical layer: a primer," *PHYDYAS, January*, 2010.

[5] D. S. Waldhauser, L. G. Baltar, and J. Nossek, "MMSE subcarrier equalization for filter bank based multicarrier systems," *Signal Processing Advances in Wireless Communications, 2008. SPAWC 2008. IEEE 9th Workshop on*, pp. 525–529, 2008.

[6] L. G. Baltar, D. S. Waldhauser, and J. A. Nossek, "MMSE subchannel decision feedback equalization for filter bank based multicarrier systems," *Circuits and Systems, 2009. ISCAS 2009. IEEE International Symposium on*, pp. 2802–2805, 2009.

[7] A. Aminjavaheri, A. Farhang, N. Marchetti, L. E. Doyle, and B. Farhang-Boroujeny, "Frequency spreading equalization in multicarrier massive MIMO," pp. 1292–1297, 2015.

[8] B. S. Chang, C. A. da Rocha, D. L. Ruyet, and D. Roviras, "On the effect of ISI in the error performance of precoded FBMC/OQAM systems," pp. 987–991, 2012.

[9] L. G. Baltar, A. Mezghani, and J. A. Nossek, "MLSE and MMSE subchannel equalization for filter bank based multicarrier systems: coded and uncoded results," pp. 2186–2190, 2010.

[10] A. Viholainen, M. Bellanger, and M. Huchard, "PHYDYAS project, deliverable 5.1: Prototype filter and structure optimization," *FP7-ICT, Tech. Rep*, 2009.